Ibn Al-Haitham Journal for Pure and Applied Sciences
Journal homepage: jih.uobaghdad.edu.iq
PISSN: 1609-4042, EISSN: 2521-3407
IHJPAS. 2026; 39(2)

Influence of Voltage Variation on Plasma Parameters in Cylindrical Electrostatic Precipitators Using Optical Emission Spectroscopy

Hadeer Adil Abbas[1,2*], and Qussay Adnan Abbas[2]
[1,2]Department of Physics, College of Science, University of Baghdad, Baghdad, Iraq
[2] Medical Technical Institute – Al-Mansour, Middle Technical University, Baghdad, Iraq
*Corresponding Author

Received: 16/August/2025
Accepted: 7/December/2025
Published: 20/April/2026
doi.org/10.30526/39.2.4282

Abstract

In this work, plasma spectroscopy was used to measure the plasma parameters of a negative spark discharge in a cylindrical electrostatic precipitator (ESP) from spectral data (electron density ne, electron temperature T_e, plasma frequency, and Debye length). The characteristics of the spark-type plasma discharge were characterized using photoemission spectroscopy (PES), and the effect of varying the voltage on the discharge characteristics was investigated using voltages of 15, 20, and 25 kV and a pressure of 252 Torr. The Stark dilation method was used to calculate the electron number density, while Boltzmann diagrams were used to calculate the electron temperature. The results show that increasing the voltage increases the electron number density and plasma frequency but decreases the electron temperature and Debye length. These results indicate that higher voltage promotes more intense ionization, reduces electrostatic shielding, and thus improves the charge-particle dynamics in Electrostatic Precipitator systems. Identifying voltage ranges that yield favorable plasma conditions can improve particle charging and maintain stable discharge.

Keywords: Cylindrical electrostatic precipitators, Negative spark discharge, Electron temperature, Electron density, Optical emission spectroscopy.

1.Introduction

Electrostatic precipitators (ESPs) are commonly employed in industrial air pollution control because of their effectiveness in capturing fine and ultrafine particles from gas streams. Among the different ESP designs, the cylindrical (tubular) configuration is particularly suitable for handling wet, sticky, or oily particulate matter, making it valuable in petrochemical and combustion-related applications. These devices operate by establishing a strong electric field between a discharge electrode and a collecting surface, causing ionization of the working gas and subsequent charging of airborne particles, which are then driven to the collector by electrostatic forces [1,2].

While many ESPs rely on a corona discharge for particle charging, spark discharges can also occur under certain operating conditions, especially at higher applied voltages .In a negative polarity spark discharge, the intense electric field near the cathode accelerates electrons to high kinetic energies, causing strong ionization and excitation of gas molecules through inelastic collisions. This results in short-lived, highly ionized plasma channels that differ noticeably from corona-generated plasmas, showing higher electron densities and increased electron temperatures [3,4].

Plasma diagnostics are essential for analyzing such discharges and for understanding their effect on ESP performance. Optical emission spectroscopy (OES) is a non-intrusive method that provides precise data on electron temperature and electron density, along with other plasma

parameters derived from these values, such as Debye length and plasma frequency. To evaluate the electron temperature (Te), the Boltzmann plot method is frequently employed by analyzing the relative intensities of selected emission lines originating from the same atomic species. In contrast, electron density (ne) is typically inferred through Stark broadening effects observed in a suitable spectral transition[5,6]. More recently, other studies explored negative corona and spark discharges in cylindrical ESPs, confirming the voltage-dependent variations in plasma characteristics [7]. Collectively, these studies reinforce the relevance of the present work and provide a strong theoretical foundation for its experimental approach.

In the present work, a cylindrical electrostatic precipitator (ESP) was operated under fixed sub-atmospheric conditions, specifically at 252 Torr, to investigate the influence of varying applied voltages (15, 20, and 25 kV) on fundamental plasma characteristics during negative spark discharges. The analysis centers on how voltage escalation modifies the excitation and ionization behavior within the plasma, subsequently impacting T_e, ne, and other interrelated parameters. Understanding these dependencies is essential for improving the functional performance of ESPs, particularly in terms of charge transfer efficiency and discharge stability under transient spark regimes.

Recently, several studies have further explored plasma behavior in electrostatic precipitators using advanced diagnostic techniques, providing additional theoretical support and context for the present investigation.

2. Materials and Methods

2.1. Theoretical Description of Discharge Parameters

The ratio approach is one of the most often used optical emission spectroscopy (OES), and the Boltzmann equation is used to identify the electron temperature as

$$\ln\left(\frac{Iji\,\lambda ji}{hc\,Aji\,gji}\right) = -\frac{Ej}{K_B T} + \ln\left(\frac{N}{U(T)}\right) \quad \textbf{(1)}$$

The term g_j refers to the high-level statistical weight associated with the transitional state, while I_{ji} denotes the relative emission line intensity between energy levels iii and j. The wavelength is represented as λ_{ji} (measured in nanometers), and E_j corresponds to the excitation energy of level j (expressed in electron volts). The parameter A_{ji} signifies the probability of a spontaneous radiation transition from level i to j. Additionally, N stands for the population density, and k_B Boltzmann's constant [8].

The left-hand side of **Equation 1** is plotted against the higher-level energy of the species in the Z ionization phase in eV units to determine the electron temperature [9,10]. The electron number density (n_e) is determined using the Stark broadening method [11]:

$$n_e = \left[\frac{\Delta\lambda}{2\omega_s}\right] N_r \quad \textbf{(2)}$$

The Stark parameter's full width is theoretically described by the spectral line w, where the electron density is estimated at approximately $Nr \approx 10^{17}$ cm^{-3}. The FWHM refers to the full width at half the maximum intensity of the spectral line[12,13]. The inverse of the slope of the Boltzmann plot is used to calculate the temperature of electrons [14].

Many plasma interactions with electromagnetic waves take place at the plasma frequency f_{pe}, which is defined as [15,16]

$$\omega_p = \sqrt{\frac{n_e e}{m_e \varepsilon_0}} \quad \textbf{(3)}$$

The Debye length (λ_D) is directly related to the square root of electron's temperature and inversely proportional to electron density[9], as

$$\lambda_D = \sqrt{\frac{\varepsilon_\circ KT_e}{n_e\, e^2}} = 743 * \sqrt{T_e / n_e} \ \text{(cm)} \quad \textbf{(4)}$$

The shielding provides the plasma with its quasi-neutrality characteristic [17,18].

2.2. Experimental Set Up

The Cylindrical Electrostatic Precipitator chamber consists of two coaxial cylindrical tubes, the outer hollow tube, which is made from aluminum and used as a collector electrode, of (28) cm in length and (4.8) cm in diameter. While the inner tube was used as a negative electrode with (37) cm in length and (0.5) cm in diameter, it was used to charge the air particles that enter the tubular electrostatic precipitator. Both electrodes are surrounded by an outer Pyrex tube. This tubular precipitator was connected to a vacuum pump (Model: VE115N, made in China) through a pressure gauge that was used to control the air pressure, as illustrated in **Figure 1.**

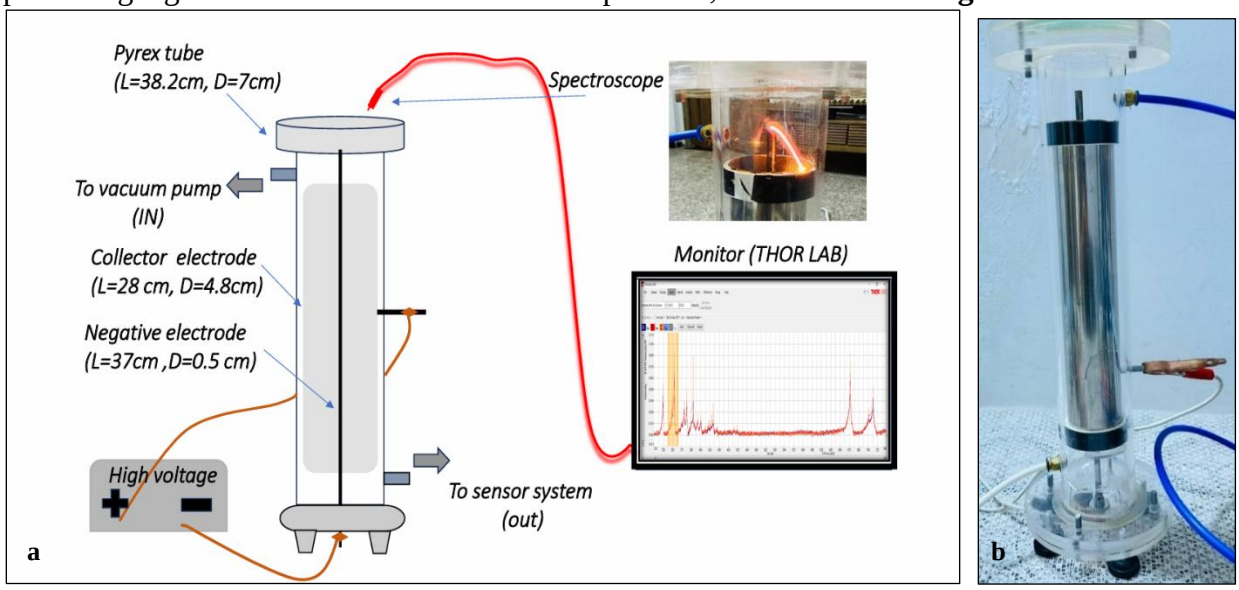

Figure1. experimental setup a, b.

3. Results

3.1. Mechanism of Spark Discharge

The onset of the negative spark discharge in the cylindrical ESP was initiated when the local electric field strength in the inter-electrode gap exceeded the breakdown threshold for air at the operating pressure of 252 Torr. Under these conditions, field-emitted electrons from the negatively charged central rod were rapidly accelerated toward the grounded collection cylinder, undergoing frequent inelastic collisions with gas molecules. This process triggered an avalanche ionization mechanism, characteristic of Townsend discharge theory [19], which rapidly transitioned into a high-current, transient plasma channel. The sub-atmospheric pressure favored longer mean free paths for the electrons, enhancing their kinetic energy before collision and resulting in increased excitation and ionization rates [20]. The subsequent collapse of the plasma channel after each spark was followed by a quenching period, during which space charge effects temporarily suppressed re-ignition until the local field recovered to breakdown strength. This repetitive cycle was found to be strongly dependent on the applied voltage, consistent with observations in previous studies on negative polarity spark discharges in wire–cylinder configurations [21,22]. Moreover, spark discharges in such configurations are characterized by brief but intense plasma events that produce elevated electron densities and temperatures compared to continuous corona discharges, significantly influencing the charging efficiency in electrostatic precipitators [23], **Figure 2**shows the spark discharge in different voltage.

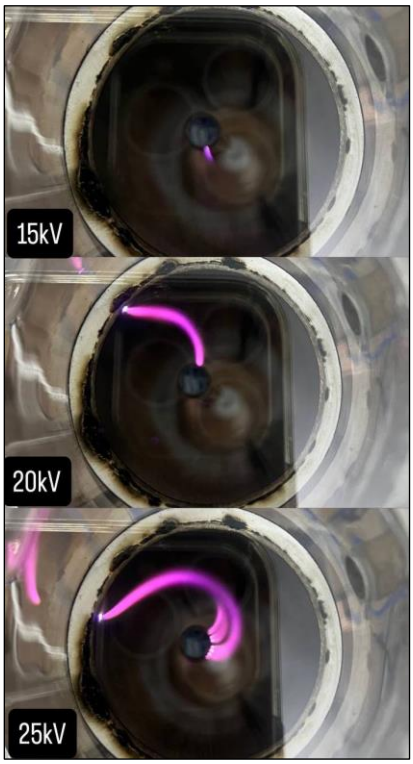

Figure 2. Images of spark discharge in an electrostatic cylinder at various voltages.

3.2. Optical Emission Spectra

An optical emission spectrometer (Thorlabs CCS100/M) was employed to analyze the emission spectra of plasma generated by spark discharge inside the electrostatic precipitator, which operated at sub-atmospheric pressure (252 Torr) and applied voltages of 15, 20, and 25 kV. Emission in the wavelength range of 320–740 nm was recorded by using a spectrum analyzer (model THOR Lab) ,and plasma parameters were determined using the NIST Atomic Spectra Database [24]. In **Table 1**, all the recorded lines in the examined spectral region are reported, and the spectroscopic data that relates.

Table 1. The NIST database of spectroscopic parameters of spectral lines generated by plasma.

Element	λ (nm)	$g_h A_{ki}$ (s^{-1})	E_i (ev)	E_k (eV)
O II	487.2017	3.74e+07	28.829685	31.373797
	667.7866	1.35e+07	28.955839	30.81197
	677.4984	1.05e+07	28.941697	30.771222
	712.8865	4.48e+07	29.0622429	30.800949
	734.6901	1.72e+07	29.0622429	30.74935

Figure 3 presents the emission spectra of spark plasma at sub-atmospheric pressure (252 Torr) for applied voltages of 15, 20, and 25 kV. The spectra exhibit multiple ionic oxygen (O II) lines at 337.0, 353.6, 357.3, 366.9, 375.2, 380.2, 427.7, 433.6, 470.1, 487.2, 667.7, 677.4, 708.3, 712.8, and 743.6 nm; nitrogen ionic (N II) lines at 391.3 and 399.49 nm; and one atomic nitrogen (N I) line at 674.1 nm. The intensity of all observed lines increases with applied voltage. The spectra indicate a higher abundance of atomic oxygen emissions compared to nitrogen, attributed to the lower ionization energy of oxygen (13.62 eV) relative to nitrogen (14.53 eV), making oxygen more readily ionized under these discharge conditions[10].

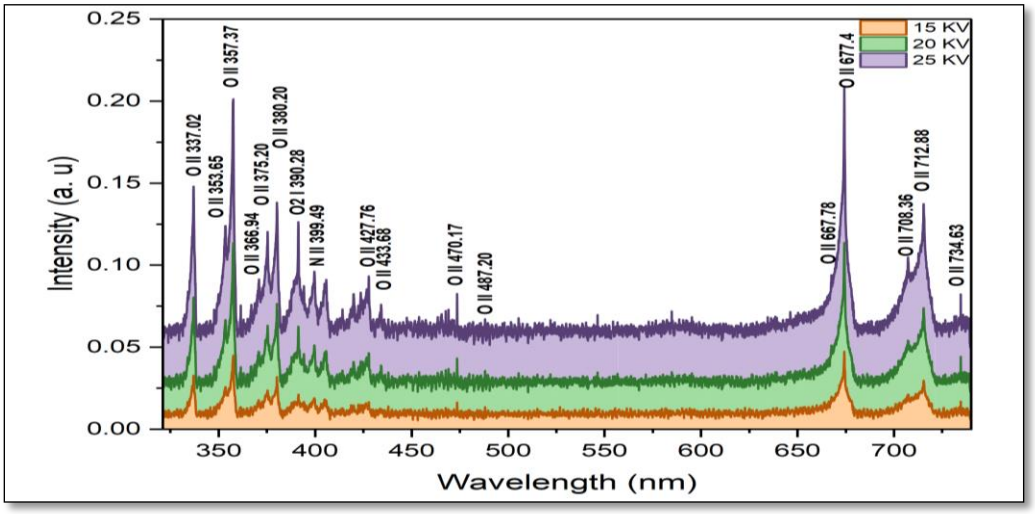

Figure 3. Emission spectra of plasma at 252Torr with various voltages.

3.3.Fundamental Discharge Characteristics

Figure 4 I–V characteristics were obtained for both negative spark discharge and positive spark discharge configurations in a cylindrical electrostatic precipitator at a fixed pressure of 252 Torr [26]. In both setups, increasing the applied voltage elevated the discharge current, indicating enhanced ionization and breakdown under stronger electric fields[25]. However, the negative spark discharge consistently produced higher currents at the same voltages compared to the positive spark discharge. This disparity reflects the intrinsic advantage of negative polarity, where the central rod acting as the high-voltage source serves as an efficient emitter of electrons that are accelerated toward the grounded outer cylinder[26]. These electrons catalyze more frequent ionizing collisions in the discharge gap, resulting in denser plasma formation.

In contrast, the positive spark discharge mode depends largely on ion-impact-induced secondary electron generation at the rod's surface, which typically yields a lower electron density and, consequently, reduced discharge current under identical conditions[27]. Given the enhanced electrical performance, increased plasma density, and improved diagnostic reliability associated with the negative spark discharge, this polarity was selected for the main body of experimental work [26].

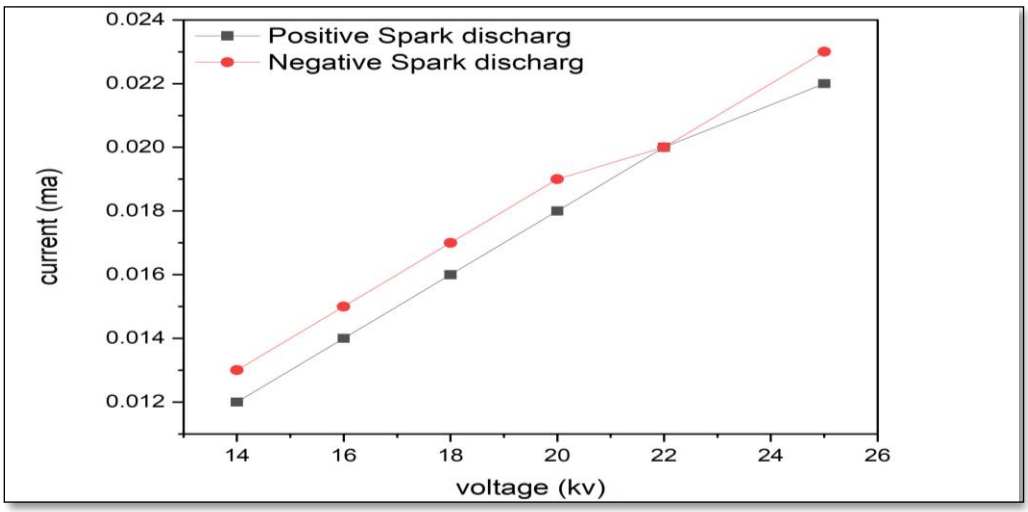

Figure 4. I–V Characteristics of Positive and Negative Spark Discharges in a Cylindrical Electrostatic Precipitator at 252 Torr

3.4. Plasma parameter

The electron temperature (T_e) and electron number density (n_e) were determined using optical emission spectroscopy (OES) at a constant sub-atmospheric pressure of 252 Torr in spark discharge conditions. The electron temperature was calculated using the Boltzmann plot method **Equation 1,** which relates the logarithm of the normalized line intensity by plotting Ln ($I_{ji}\lambda_{ji}$/hc g_jA_{ji}) against the upper energy level (E_j) for spectral lines of the same atomic species, as provided by the NIST Atomic Spectra Database [30]. The reciprocal of the slope of the best-fit line yields T_e, assuming local thermodynamic equilibrium (LTE). **Figure 5** shows the Boltzmann plots constructed from selected oxygen emission lines (O I and O II) at applied voltages of 15, 20, and 25 kV.

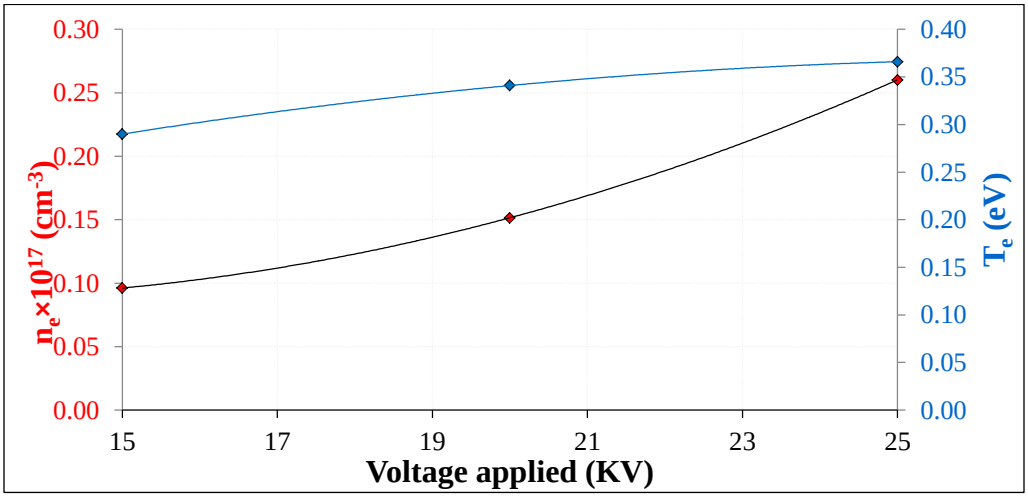

Figure 5. The variation of T_e and n_e versus the applied voltage

The electron number density (n_e) was determined from the Stark broadening of the O II spectral line at 433.68 nm using **Equation 2** and the standard broadening parameter corresponding to Nr=1×10^{17} cm^{-3} [28]. The measured Full Width at Half Maximum (FWHM) values were 0.669 nm, 1.054 nm, and 1.810 nm for applied voltages of 15, 20, and 25 kV, respectively. **Figure 6** shows the variation of T_e and n_e with applied voltage. The results indicate that T_e increases from 0.290 eV to 0.366 eV, while n_e increases from 0.096×10^{17} cm^{-3} to 0.260×$10^{17}$$cm^{-3}$ as the voltage rises from 15 to 25 kV. This trend is attributed to the higher electric field strength at increased voltages, which accelerates electrons to greater kinetic energies, enhancing the frequency of ionizing collisions and producing more free electrons.

Figure 7 illustrates the variation in Debye length (λ_D) and plasma frequency (f_p) as a function of the applied voltage ranging from 15 to 25 kV, under a constant pressure of 252 Torr in a negative spark discharge regime within an electrostatic precipitator. As the applied voltage increased, a clear inverse trend was observed in the Debye length. Specifically, λ_D decreased from 12.902 × 10^{-6} cm at 15 kV to 8.812 × 10^{-6} cm at 25 kV, representing an exact 31.7% decrease. This decline indicates that higher voltages led to a denser plasma, as increased ionization reduced the spatial extent over which electric fields are shielded [29]. In contrast, the plasma frequency exhibited a strong positive correlation with voltage. The measured values increased from 2.785 × 10^{12} Hz at 15 kV to 4.581 × 10^{12} Hz at 25 kV, corresponding to a 64.5% increase. This suggests that the plasma becomes significantly more conductive and reactive with increasing voltage due to a higher concentration of free electrons [10].

These results confirm that increasing the voltage enhances the degree of ionization, driving the plasma into a denser and more dynamic state [34]. The simultaneous decrease in Debye length and increase in plasma frequency signify a transition toward a more intense discharge regime, facilitating faster and more efficient breakdown, as typically observed in high-pressure spark environments [34]. These findings are in line with earlier studies that examined voltage-driven changes in plasma behavior within electrostatic systems [29,34].

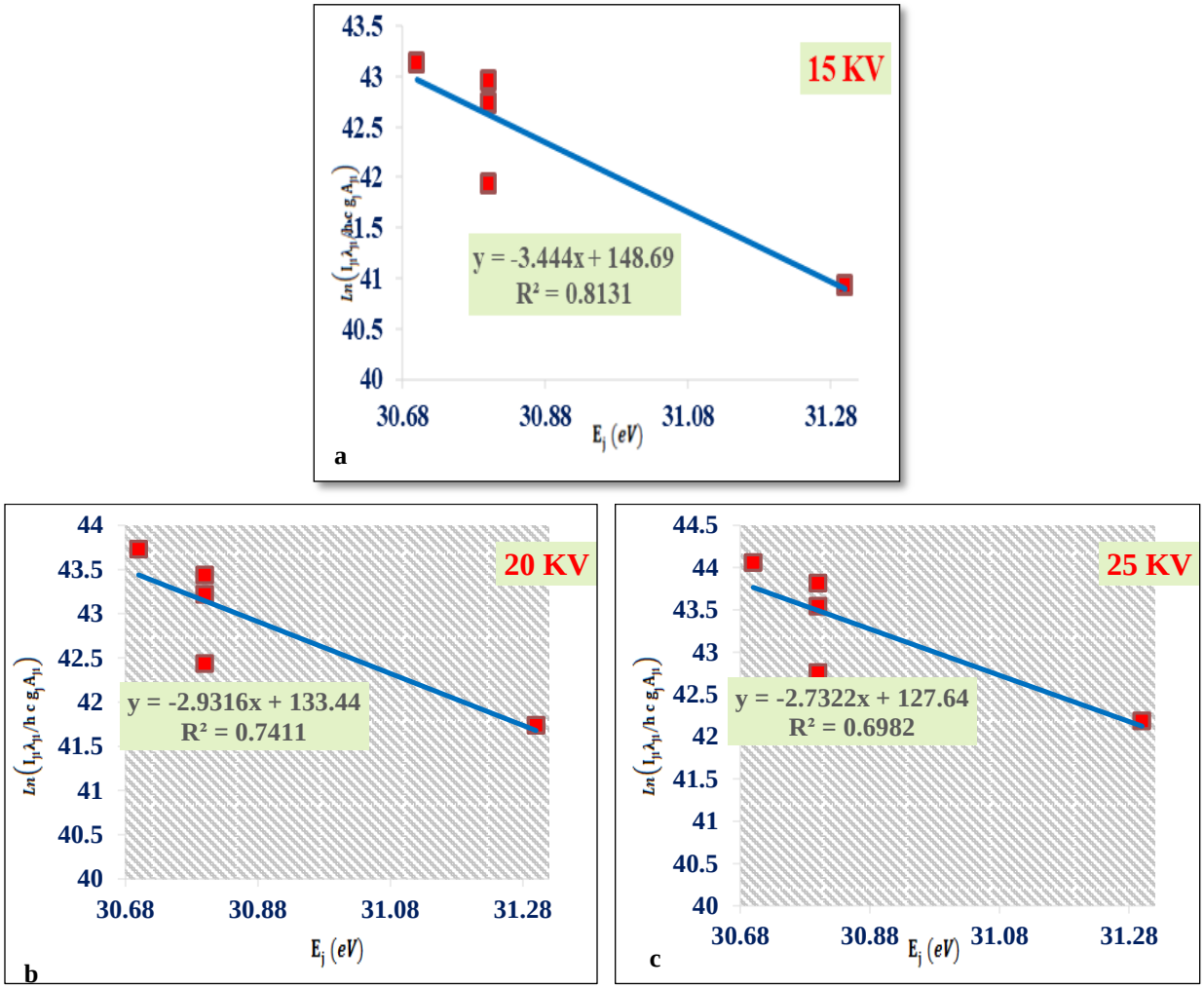

Figure 6. Boltzmann diagram of corona plasma emission from (ESPs) at different applied voltages of a:15,b: 20, and c:25 KV

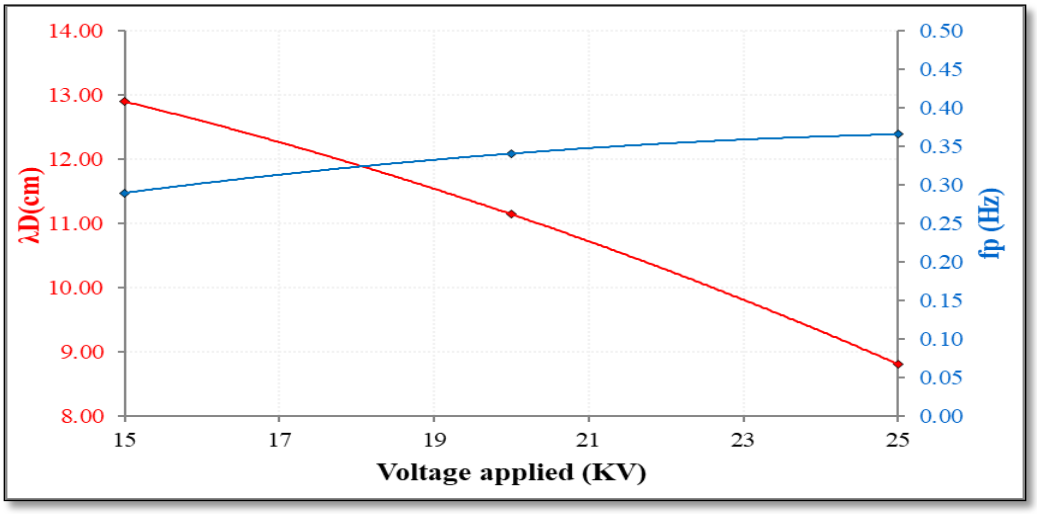

Figure 7. Variation of Debye Length and Plasma Frequency with Applied Voltage in a Negative Spark Discharge at 252 Torr

The **Table 2** shows the calculated values of parameter for spark plasma at different voltages. The plasma temperature can be calculated from **Figure 6** (R^2 represents a statistical coefficient indicating the quality of linearity).

Table 2. Plasma parameters at various voltages.

V(KV)	*T_e (eV)*	*FWHM (nm)*	*$n_e \times 10^{17}$ (cm^{-3})*	*f_p (Hz)$\times 10^{12}$*	*$\lambda_D \times 10^{-6}$(cm)*
15	0.290	0.669	0.096	2.785	12.902
20	0.341	1.054	0.152	3.495	11.147
25	0.366	1.810	0.260	4.581	8.812

4. Discussion

Measuring plasma parameters with optical emission spectroscopy (OES) in the cylindrical electrostatic precipitator (ESP) under negative spark discharge conditions offers vital insights into the plasma's physical characteristics and its interaction with particulate matter. Optical emission spectroscopy (OES) serves as a precise diagnostic tool for quantifying both electron temperature and electron density, which are critical for characterizing discharge dynamics and tracking their evolution over successive spark pulses [28]. These parameters play a pivotal role in determining the efficiency of particle charging and collection, particularly for fine and ultrafine aerosols, as they influence fundamental plasma characteristics such as the Debye length and plasma frequency [32] By capturing transient and rapid fluctuations in the plasma between spark events, OES enables fine-tuning of the applied voltage to ensure stable discharge conditions and to mitigate electrode wear over time [33]. Furthermore, shifts in plasma conductivity and density induced by changes in voltage, as revealed through spectroscopic measurements, offer actionable insights for enhancing ESP performance and operational stability, especially under reduced-pressure conditions [34].The observed results in this investigation align well with prior experimental and simulation-based studies of cylindrical electrostatic precipitators operating with negative spark discharges. For instance, employed time-resolved OES to show that repetitive negative spark discharges at sub-atmospheric pressures substantially increase electron density while simultaneously reducing the Debye length as the applied voltage is elevated [2].

Similarly, reported that intensified electric fields in negative polarity discharges compress the plasma sheath, thereby increasing the responsiveness of charged particle motion within ESPs[35]. further confirmed that voltage escalation in transient micro discharge leads to marked enhancements in plasma oscillation frequencies, consistent with the increase in f_p from 2.785×10^{12} Hz to 4.581×10^{12} Hz observed in the present work [23]. More recently, experimentally modeled wire-to-multicylinder ESPs and verified that negative DC operation yields higher discharge currents and improved particle charging efficiency compared to positive operation, in line with the present findings [36]. These consistencies across multiple independent investigations reinforce the robustness of the voltage-dependent compression of the Debye length and enhancement of plasma frequency measured in this study.

The results of this study offer practical guidance for improving the performance of cylindrical electrostatic precipitators (ESPs) under spark discharge. The observed reduction in Debye length and increase in plasma frequency with higher voltage directly support enhanced charging of fine and ultrafine particles, which is crucial for efficient pollutant removal in industrial settings.

Moreover, optical emission spectroscopy (OES) provides real-time insights into plasma behavior, enabling proactive voltage adjustments and predictive maintenance. This approach not only stabilizes discharge and reduces electrode wear but also improves energy efficiency and extends system lifespan. Integrating plasma diagnostics into ESP control systems may further ensure consistent operation across varying industrial conditions.

5. Conclusion

This study presents a detailed analysis of negative spark discharges in a cylindrical electrostatic precipitator (ESP) at sub-atmospheric pressure (252 Torr) using optical emission spectroscopy (OES). Results indicate that higher applied voltages intensify ionization, producing denser plasma and stronger electron oscillations reflected by reduced Debye length and increased plasma frequency.

These findings not only align with established discharge theory but also provide guidance for optimizing ESP performance. Identifying voltage ranges that yield favorable plasma conditions can improve particle charging and maintain stable discharge. Additionally, the use of OES highlights its value as a real-time, non-intrusive diagnostic tool for managing plasma-based filtration systems.

Acknowledgment

The authors would like to thank the department for providing the basic infrastructure required for this research.

Conflict of Interest

The authors declare that they have no conflicts of interest.

Funding

No external funding was received for this work.

Ethical Clearance

All experimental procedures were performed in accordance with the ethical standards of the University of Baghdad Research Council.

References

1. Nijdam S, van Veldhuizen E. An introduction to nonequilibrium plasmas at atmospheric pressure. Wiley; 2012. https://doi.org/10.1002/9783527649525#page=18
2. Kläusler O, Pietschnig R. Spark ablation as a versatile method for nanoparticle generation. Adv Colloid Interface Sci. 2022; 305: 102696. https://doi.org/10.1016/j.cis.2022.102696
3. Bilik N. Characterization of dust-plasma interactions in non-thermal plasmas under low pressure and atmospheric pressure [Master's thesis]. University of Minnesota; 2016. https://conservancy.umn.edu/bitstreams/a6e3cb10-e0f9-48b1-97de-f34ee58359be/download
4. Ziedan H, Tlustý J, Mizuno A, Sayed A and Ahmed A. Corona current–voltage characteristics in wire-duct electrostatic precipitators: Theory versus experiment. Int J Plasma Environ Sci Technol. 2010, 4, 154–162.
5. Tabrizi NS, Ullmann M, Vons VA, Lafont U. Generation of nanoparticles by spark discharge. J Nanopart Res. 2009;11:315–332. https://doi.org/10.1007/s11051-008-9407-y
6. Magid H. Chasib, Waleed J. Mhana, & Hanaa S. Sabaa. Spectroscopic Diagnostic of Laser-Induced Zn Plasma. Ibn Haitham J Pure Appl Sci. 2023, 36(4), 188–196. https://doi.org/10.30526/36.4.3049
7. Bas-Calopa P, Riba J R and Moreno-Eguilaz M. Corona discharge characteristics under variable frequency and pressure environments. Sensors. 2021; 21(19): 6676.
8. Noori AS, Aadim KA, Hussein AH. Characterization of discharge in ESP. Iraqi J Sci. 2022;63:2461. https://doi.org/10.24996/ijs.2022.63.7.3
9. Wasfi A S, Al-Khafaji A K, Al-Jubouri A M and Abdul-Hassan Z. H. Characterization of argon plasma induced by simple 2.45 GHz microwave source. Int Rev Phys. 2013, 7(1), 65–69.
10. Abbas ZM, Abbas QA. Influence of gas pressure on the magnetized plasma parameters of laser-induced breakdown. Opt Quantum Electron. 2023;55(10):899. https://doi.org/10.1007/s11082-023-04992-2
11. Mazhir S N. Spectroscopic study of (TiO_2)_{1-x}(CuO)_x plasma generated by Nd:YAG laser. ARPN J Eng Appl Sci. 2018, 13(3): 864–869.
12. Qasim SA, Mazhir SN. Optical emission in corona discharges. AIP Conf Proc. 2023;2475. https://doi.org/10.1063/5.0118265
13. Jaworek A, Krupa A, Czech T.. Modern electrostatic devices and methods for exhaust gas cleaning: modeling of discharge characteristics in ESP systems. J Electrostat. 2007, 65(3):133–144. https://doi.org/10.1016/j.elstat.2006.07.008
14. Inan US, Gołkowski M. Principles of plasma physics for engineers and scientists. Cambridge: Cambridge University Press; 2010. https://doi.org/10.1017/CBO9780511841225
15. Abdulhamed AS, Abbas QA. Analysis of ESP spark plasma. Iraqi J Phys. 2024;22:106.

https://doi.org/10.30723/ijp.v22i51.234
16. Chen FF. Introduction to plasma physics and controlled fusion. USA: Springer; 1984. https://doi.org/10.1007/978-1-4757-5595-4
17. Chen FF. Introduction to plasma physics. USA: Springer; 2012. https://doi.org/10.1007/978-1-4614-7382-7
18. Zhang B, Aravind I, Yang S, Weng S, Zhao B, Schroeder C, Schroeder W, Thomas M, Umstattd R, Singleton D, Sanders J, Heejung J. Plasma-enhanced electrostatic precipitation of diesel exhaust particulates using nanosecond high-voltage pulse discharge for mobile source emission control. Sci Total Environ. 2022; 851: 158181.. DOI: 10.1016/j.scitotenv.2022.158181
19. Xiao D. Fundamental theory of Townsend discharge. In: Gas Discharge and Gas Insulation. Springer; 2016. https://doi.org/10.1007/978-3-662-48041-0_3
20. Gallagher TF, Dunning FB. Mean free paths and collision processes in low-pressure plasmas. J Appl Phys. 1985;58(1):22–28. https://doi.org/10.1063/1.336312
21. Xin H, Yang G, Wei H, Zhang L. Experimental study on electrostatic spark discharge under different pressures. J Electrostat. 2023;103:103731. https://doi.org/10.1016/j.elstat.2023.103731
22. Yang B.Experimental study on plasma channel formation with spark discharges in high-current pulsed electron beam source. Vacuum. 2023; 207: 111649.
23. Staack D, Farouk B, Gutsol A, Fridman A. Characterization of a DC atmospheric pressure normal glow discharge. Plasma Sources Sci Technol. 2005;14(4):700–711. https://doi.org/10.1088/0963-0252/14/4/009
24. Greda K, Dors M, Mizeraczyk J. Optical emission spectroscopy diagnostics of spark discharge plasma in air. Journal of Physics D: Applied Physics. 20215;l4(12):125202. https://doi.org/10.1088/1361-6463/abda0f
25. Chen G, Zhao Y, Li H, Yu J. Comparison of corona and spark discharge modes in an electrostatic precipitator. IEEE Trans Dielectr Electr Insul. 2014;21(2):875–882. https://doi.org/10.1109/TDEI.2014.004356
26. Lu X, Reuter S, Laroussi M, Liu D. Nonequilibrium Atmospheric Pressure Plasma Jets: Fundamentals, Diagnostics, and Medical Applications. CRC Press; 2019. https://doi.org/10.1201/9780429053665
27. Turner M. M. Kinetic modeling of low-pressure plasmas using Particle-in-Cell/Monte Carlo collision methods.J Phys D Appl Phys. 2013, 46(19), 193001. https://doi.org/10.1088/0022-3727/46/19/193001
28. Sherbini A, Al Aamerv A A S , A T Hassan. Measurements of Plasma Electron Temperature Utilizing Magnesium Lines Appeared in Laser Produced Aluminum Plasma in Air. Opt Photonics J. 2012; 2(4): 278–285. DOI: 10.4236/opj.2012.24034
29. Mermigkas CG. Simulation of electrostatic precipitator performance under varying electrical and flow conditions. Int J Environ Sci Technol. 2016;13(1):59–68. https://doi.org/10.1007/s13762-015-0872-2
30. Oglesby S, Nichols GB. Electrostatic precipitators. Marcel Dekker; 2014. https://doi.org/10.1201/9781482274747
31. Kohut A, Beňo J, Kudela T, Zahoranová A, Kováčik D. Optical emission spectroscopy of transient spark discharge in atmospheric air. Nanotechnology. 2017;28(45):455705. https://doi.org/10.1088/1361-6528/aa8f84
32. Lee J. Characterization of particle charging mechanisms in electrostatic precipitators using optical diagnostics [Doctoral dissertation]. University of Illinois at Urbana-Champaign; 2019. https://search.proquest.com/openview/42ebc25c2acd58c22733e56aa00ad795
33. Zaplotnik R, Vesel A, Mozetic M, Primc G. Diagnostics of transient plasma discharges: From breakdown to afterglow. Appl Sci. 2021;11(5):2275. https://doi.org/10.3390/app11052275
34. Hensel K, Katsurayama H, Mizuno A. Generation of streamer discharges in humid air and their influence on removal of fine particles in an electrostatic precipitator. Plasma Process Polym. 2007;4(7–8):682–693. https://doi.org/10.1002/ppap.200700022
35. Czech T, Sobczyk AT, Jaworek A. Optical emission spectroscopy of point-plane corona and back-corona discharges in air. Eur Phys J D. 2011;63:369–381. https://doi.org/10.1140/epjd/e2011-20196-x
36. Krachai BK. Experimental modelling of wire-to-multicylinder electrostatic precipitator. Appl Sci. 2020;10(10):34–42. https://doi.org/10.15199/48.2020.10.34